International Symposium
On Turbulence and Shear Flow
Phenomena (TSFP-8)
August 28 - 30, 2013 Poitiers, France

SQUARE-FRACTAL-ELEMENT GRID-GENERATED TURBULENCE

R. Jason Hearst & Philippe Lavoie
Institute for Aerospace Studies
University of Toronto
Toronto, Canada, M3H 5T6
lavoie@utias.utoronto.ca

ABSTRACT

A new square-fractal-element grid was designed to investigate the decay of turbulent kinetic energy far downstream of a fractal geometry. The grid is composed of several square fractal elements mounted to a background mesh. Measurements of the decay of turbulent kinetic energy at $Re_{L_0} = 57{,}000$ in the region $23 \leq x/L_0 \leq 45$, where L_0 is the size of the largest element in the grid, yield a power-law decay of the form $\langle q^2 \rangle \sim (x - x_0)^m$ with $m = -1.39$. This result agrees with values of m previously reported for regular grids, while it contrasts with $m \approx -2.5$ previously reported for space-filling square fractals (Valente & Vassilicos, 2011). It is also observed that Richardson-Kolmogorov scaling, both for the spectra and for C_ε, approximately describes the turbulence produced by this new grid. This is also in agreement with previous regular grid experiments, but contrasts with previous fractal grid experiments. Previous fractal studies have been conducted in the region $x/L_0 < 20$, and thus the contrasting results are attributed primarily to the difference in measurement region relative to L_0 of the present and previous studies.

INTRODUCTION

Grid turbulence is an ideal empirical platform for the evaluation of turbulence theories and models because it produces flow that approximates homogeneous, isotropic turbulence (HIT) and transforms the temporal decay of turbulence into a spatial one. This decay is typically believed to follow the form $\langle q^2 \rangle \sim (x - x_0)^m$, where $\langle q^2 \rangle = \langle u^2 \rangle + \langle v^2 \rangle + \langle w^2 \rangle$ is twice the turbulent kinetic energy, x is downstream distance, and x_0 is a virtual origin. Since the seminal work of Comte-Bellot & Corrsin (1966), exponent values ranging $-1 \gtrsim m \gtrsim -1.4$ have been reported (Mohamed & LaRue, 1990; Lavoie *et al.*, 2007; Krogstad & Davidson, 2010, 2011).

The work of Hurst & Vassilicos (2007) has catalyzed a modern resurgence in grid turbulence research (Mazellier & Vassilicos, 2010; Valente & Vassilicos, 2011; Krogstad & Davidson, 2010, 2011, 2012). Vassilicos and co-workers have found that the decay behind space-filling square fractals is very rapid, $m \approx -2.5$ (Valente & Vassilicos, 2011). They also observed that the streamwise integral length scale was approximately proportional to the Taylor microscale, i.e. $L_u/\lambda \approx$ constant, and that the turbulence may be described by a single-length-scale, as normalization by large scale variables collapsed the spectra at all wavenumbers (which is atypical of regular grid turbulence experiments). Vassilicos and co-workers have linked this form of rapid decay to a possible breakdown of the traditional dissipation scaling, $\varepsilon \sim \langle q^2 \rangle^{3/2} / L_u$.

To date, fractal studies have employed 'space-filling' square fractals where a single fractal element occupies the entire wind tunnel cross-section. In such a setup, the largest element of the grid, with length L_0, is approximately half the tunnel height, H, i.e. $H/L_0 < 2$. Corrsin (1963) states that for reasonable homogeneity, $H/M \gg 1$, where M is the mesh length of the grid. If the largest scale induced by a square fractal grid is of order L_0, making it roughly equivalent to M for a regular grid, then Corrsin's criterion is not satisfied for the space-filling square fractals. This may have a negative impact on the approximation of HIT by the flow (Wang & George, 2002). Furthermore, given the size of L_0, the relative downstream distance is limited, e.g. $x/L_0 < 20$ in previous studies.

In order to reconcile the rapid decay results of Valente & Vassilicos (2011) with previous measurements, Krogstad & Davidson (2011) designed and tested multi-scale 'cross' grids that consisted of a regular square mesh with alternating bars of different thickness. Their results demonstrated that the cross grid multi-scale turbulence did decay with traditional values between $-1.12 \geq m \geq -1.25$. Later, Krogstad & Davidson (2012) performed measurements in the near-grid region of their cross grids and discovered that the flow was similar to that produced downstream of a square fractal. However, previous work has not specifically addressed how square fractal-generated turbulence behaves in the far-field. In fact, Valente & Vassilicos (2011) suggest that if a multi-scale grid was designed such that the wakes of the various elements could interact in a relatively short distance, citing specifically cross grids, that it is likely that the produced turbulence would be similar to that produced by a regular grid. In the present work, a new design strategy, where a small fractal element is repeated several times, is implemented in order to increase H/L_0. This strategy both improves the transverse homogeneity and extends the downstream range relative to L_0, addressing the limitations of earlier fractal work while preserving the fractal geometry.

EXPERIMENTAL PROCEDURE

The new square-fractal-element grid is composed of several $N = 3$ square-fractal-elements (where N is the number of times the fractal shape is repeated) mounted to a background grid with mesh length $M = L_0 = 100$ mm and thickness $t_0 = 6.7$ mm (see figure 1). The fractal elements

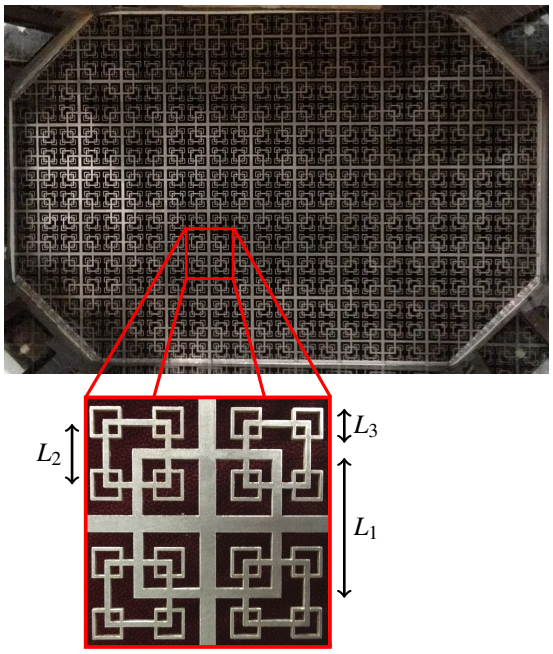

Figure 1. Square-fractal-element grid positioned *in situ* (left) with a blow-up of a single fractal element (right) and labels defining dimensions.

have lengths $L_i = 55.6, 24.7$, and 11.0 mm with thicknesses $t_i = 4.1, 2.5$, and 1.5 mm. The factors by which the length and thickness were incremented for each fractal iteration were $R_L = 2.25$ and $R_t = 1.65$, respectively. The solidity of the grid is $\sigma = 0.39$. The grid was laser cut out of a single sheet of 3 mm thick stainless steel.

Measurements were performed in the low-speed closed-loop wind tunnel at the University of Toronto Institute for Aerospace Studies. The wind tunnel has a background turbulence intensity of 0.05% for $U \leq 13$ m/s. The test-section is 5 m long and has a cross-sectional area of 1.2 m $\times$ 0.8 m. The corners of the test-section are adjustable and were used to create a zero pressure gradient over its length, such that $U = 9$ m/s $\pm 1\%$ was maintained throughout the test-section, corresponding to $Re_{L_0} = UL_0/\nu = 57{,}000$. Data were acquired with both single-wire and X-wire probes simultaneously. The wires were prepared in-house using 2.5 μm thick copper-coated tungsten mounted to Dantec-style prongs. All sensing lengths were maintained at $\ell = 0.65 \pm 0.05$ mm. Over the range of Kolmogorov scales η $(\equiv \nu^{3/4}/\langle\varepsilon\rangle^{1/4})$ measured, the resolution of the probes was $1.4 \lesssim \ell/\eta \lesssim 2.3$. The hot-wires were calibrated *in situ* at the farthest downstream location, where the turbulence intensity was less than 1%. The single-wire was calibrated with ten velocities fit with a fourth-order polynomial. The X-wires were calibrated with ten velocities and seven angles, using the look-up table approach described by Burattini & Antonia (2005). Pre- and post-calibrations were performed for every set of streamwise measurements to account for hot-wire drift. Prior to acquisition, data were low-pass filtered at 9.2 kHz with the sampling frequency set to twice that of the filter. Samples were recorded for 8 minutes or longer in order to ensure better than $\pm 1\%$ convergence of $\langle q^2 \rangle$, which was estimated from $\langle q^2 \rangle = \langle u^2 \rangle + 2\langle v^2 \rangle$ after verifying $\langle v^2 \rangle \approx \langle w^2 \rangle$. In the streamwise direction, measurements were performed in 32.0 mm ($\approx L_0/3$) increments in the range 2.3 m $\leq x \leq$ 4.5 m using a stepper-motor-actuated traverse. This range is farther downstream than the work of Vassilicos and co-workers and does not overlap with their measurement region due to mechanical limitations of the traverse. Vertical profiles were also measured at $x = 2.4$ m and 3.27 m over the range -17.5 cm $\leq z \leq 10$ cm in increments of 24.0 mm ($\approx L_0/4$).

Post-acquisition, data were recursively band-pass filtered between 1.25 Hz and the Kolmogorov frequency, $f_K = U/2\pi\eta$, using the technique introduced by Mi *et al.* (2011). A fifth-order digital Butterworth filter was used. Gradients were estimated using a sixth-order centred-difference scheme, and spatial corrections were made for both the fluctuating velocities and gradients (Wyngaard, 1968; Zhu & Antonia, 1995; Hearst *et al.*, 2012).

RESULTS

Homogeneity and isotropy

Table 1 presents estimates of several turbulence properties at five discrete downstream locations. The values of u'/v', which represent the global isotropy, presented in table 1, are in good agreement with previous passive grid turbulence measurements (Comte-Bellot & Corrsin, 1966; Hurst & Vassilicos, 2007; Lavoie *et al.*, 2007; Krogstad & Davidson, 2010, 2011). Furthermore, the degree of local isotropy exhibited by the flow is also very good with $\langle(\partial v/\partial x)^2\rangle/\langle(\partial u/\partial x)^2\rangle \geq 1.75$, where 2 is the ideal case. For perspective, Valente & Vassilicos (2011) measured local isotropy values below 1.5.

Corrsin (1963) states that 'some necessary conditions for effective homogeneity are':

$$\frac{\mathrm{d}L_u}{\mathrm{d}x} \ll 1, \quad \frac{L_u}{\lambda}\frac{\mathrm{d}\lambda}{\mathrm{d}x} \ll 1, \quad -\frac{L_u}{\langle u^2\rangle}\frac{\mathrm{d}\langle u^2\rangle}{\mathrm{d}x} \ll 1, \qquad (1)$$

where L_u is the integral length scale based on u. Here, L_u is estimated by integrating the area under the autocorrelation, $\langle u(x)u(x+r)\rangle$, to the first zero-crossing. These quantities are plotted with offsets in figure 2(a) and are all shown to be relatively constant and very close to zero. Further assessment of the homogeneity may be made by estimating the skewness, S_u, and flatness, F_u, of the probability density functions of u. Figure 2(b) demonstrates that $S_u(x)$ approaches zero downstream, as is typical in grid turbulence. Furthermore, $F_u(x)$ is independent of x and has a mean value of ≈ 2.95, again in good agreement with previous measurements and expectations (Krogstad & Davidson, 2011). Figure 2(c), which shows the transverse measurements of $S_u(z)$ and $F_u(z)$, verifies that they are approximately constant in the two planes measured. Finally, the ratio of L_u/L_v is approximately constant with x/L_0 (see table 1), indicating the relative size of the largest eddies in the two directions remains constant throughout the decay.

Power-law decay

The power-law decay of turbulent kinetic energy may be expressed as

$$\langle q^2 \rangle = A\left(\frac{x}{L_0} - \frac{x_0}{L_0}\right)^m, \qquad (2)$$

x/L_0	25.0	30.0	35.0	40.0	44.5	
$\langle u^2\rangle^{1/2}\lambda/\nu = Re_\lambda$	99	92	89	85	82	
u'/U	3.11	2.65	2.35	2.12	2.00	[%]
L_u	31.9	33.9	36.3	36.9	37.9	[mm]
$\left[5\nu\langle q^2\rangle/\langle\varepsilon\rangle_d\right]^{1/2} = \lambda$	5.4	6.0	6.6	7.1	7.6	[mm]
η	0.29	0.33	0.37	0.41	0.44	[mm]
$-(U/2)(\mathrm{d}\langle q^2\rangle/\mathrm{d}x) = \langle\varepsilon\rangle_d$	0.59	0.34	0.22	0.15	0.11	[m^2 s^{-3}]
$3\nu\left[\langle(\partial u/\partial x)^2\rangle + 2\langle(\partial v/\partial x)^2\rangle\right] = \langle\varepsilon\rangle_{XW}$	0.63	0.37	0.24	0.16	0.13	[m^2 s^{-3}]
$15\nu\langle(\partial u/\partial x)^2\rangle = \langle\varepsilon\rangle_{iso}$	0.66	0.39	0.26	0.18	0.14	[m^2 s^{-3}]
u'/v'	1.13	1.13	1.16	1.16	1.17	
$\langle(\partial v/\partial x)^2\rangle/\langle(\partial u/\partial x)^2\rangle$	1.89	1.87	1.78	1.75	1.77	
L_u/L_v	2.4	2.4	2.4	2.3	2.3	

Table 1. Turbulent flow properties at five downstream locations.

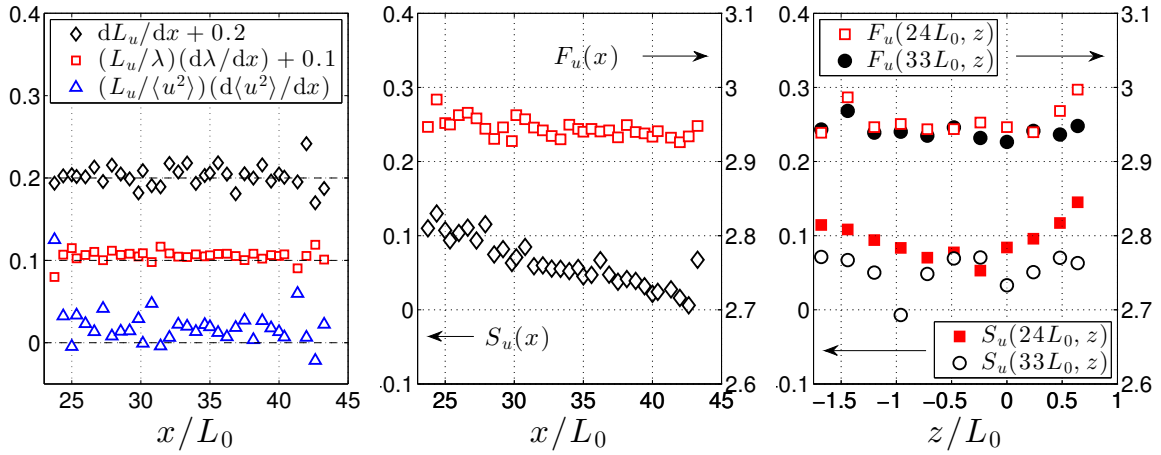

(a) (b) (c)

Figure 2. Assessment of flow homogeneity. (a) Corrsin (1963) streamwise homogeneity criteria. (b) Streamwise direction skewness and flatness. (c) Transverse plane skewness and flatness. Only every second point is plotted in order to reduce clutter in (a) and (b).

where A is a constant of proportionality, x_0 is a virtual origin, and L_0 is used to non-dimensionalize x. The typical choice for non-dimensionalizing x is M, however this is not applicable here. It is common to use a least-squares method to fit empirical measurements of $\langle q^2\rangle$ to (2). Mohamed & LaRue (1990) remarked that the accuracy of the least-squares fitting is greatly improved if the number of variable parameters is reduced. Rather than treating x_0 as a free parameter, Lavoie *et al.* (2007) developed a technique where a range of x_0 values were inserted into the power-law, and A and m were determined with less variance for each x_0. There is also significant ambiguity associated with identifying $x_{\min}$, which marks the beginning of the power-law decay range (PLDR). Determining $x_{\min}$ has been addressed in several ways in previous studies, but typically it is accepted that measurements recorded in the range $x/M \gtrsim 30$ are within the PLDR (Corrsin, 1963; Comte-Bellot & Corrsin, 1966; Lavoie *et al.*, 2007; Krogstad & Davidson, 2011).

The technique used here is a combination of that proposed by Lavoie *et al.* (2007) and the regression technique of Krogstad & Davidson (2011). The present technique is aimed at reducing ambiguities associated with user choice in the power-law fitting process. The technique is as follows:

1. A linear fit is made to the natural logarithm of (2) for virtual origins over a range $-8.0 \le x_0/L_0 \le 13.0$ in increments of 0.5 using a least-squares regression algorithm. For each x_0/L_0, the power-law is also estimated for various $x_{\min}/L_0$ values starting from the first measurement location. Fits are not made to ranges smaller than $10L_0$ due to a rapid decrease in fitting accuracy. Through this process, a matrix of m values is created where one dimension represents the dependence of m on x_0/L_0 and the other on $x_{\min}/L_0$.
2. The virtual origin is selected by choosing the x_0/L_0 which yields the lowest standard deviation of m relative to its mean for all choices of $x_{\min}/L_0$. This has the effect of choosing the x_0/L_0 which is least influenced by the PLDR, indicating that the power-law is constant over the largest downstream range.
3. Given x_0/L_0 from step (2), the normalized root-mean-square deviation (χ) is then calculated between the data and the power-law fit for each possible choice of

$x_{\min}/L_0$. $x_{\min}/L_0$ is then chosen such that χ is minimized. Through this process, the PLDR represents the power-law range that fits the data most accurately.

4. The percentage difference (Δ_i) is then calculated at each measurement location between $\langle q^2 \rangle$ and the power-law fit obtained from step (3). Steps (1), (2), and (3) are then repeated iteratively, excluding from the fitting process any locations i where Δ_i is outside of two standard deviations from its mean. The end criterion is that no outliers are detected.

The above technique was applied to the streamwise measurements of $\langle q^2 \rangle$ for the square-fractal-element grid. The process converged in two iterations and only discarded 4 out of 70 measurements. The estimated power-law that describes the empirically measured $\langle q^2 \rangle$ is $\langle q^2 \rangle = 12.81\,(x/L_0 - 6.0)^{-1.39}$ and applies over the range $24.1 \leq x_0/L_0 \leq 45$ with $\chi = 1.11\%$. Figure 3(a) plots the decay of $\langle q^2 \rangle$ and its fit. Figure 3(b) shows the variation of m with $x_{\min}/L_0$ for different values of x_0/L_0. The error bars indicate the value of χ for each fit. The uncertainties on the power-law parameters are $x_0/L_0 \pm 2$, $x_{\min}/L_0 \pm 1$, and $m \pm 0.1$. These relatively high uncertainties compared to previous regular grid experiments are attributable to the relatively short decay range investigated here. However, the range over which the power-law is fitted here is significantly longer than any other previous fractal grid experiments.

To gain confidence in the estimate of m, it is common to estimate the power-law based on $\langle u^2 \rangle$ and $\langle v^2 \rangle$ separately, but using the values of x_0/L_0 and $x_{\min}/L_0$ found for $\langle q^2 \rangle$. This also ensures that the results are self-consistent. Values of $m_u = -1.32$ and $m_v = -1.44$ were found for the decay of $\langle u^2 \rangle$ and $\langle v^2 \rangle$, respectively. These are both within $\pm 5\%$ and the uncertainty of m estimated from $\langle q^2 \rangle$. The classical behaviour experienced within the present measurement region is further validated by the approximately linear evolution of λ^2, figure 3(a), which is a consequence of the power-law decay (George, 1992; Danaila *et al.*, 2002).

Significantly, the values of m found here are closer to the regular grid results reported in the literature than to $m \approx -2.5$ found in earlier fractal work. Furthermore, the value of $x_{\min}/L_0 = 24.1$ is in good agreement with typical values of $20 \lesssim x_{\min}/M \lesssim 35$ for regular grids if L_0 is assumed to be equivalent to M (Comte-Bellot & Corrsin, 1966; Lavoie *et al.*, 2007; Krogstad & Davidson, 2011). It is also worth noting that this value of $x_{\min}/L_0$ is beyond the farthest downstream point of previous fractal grid measurements.

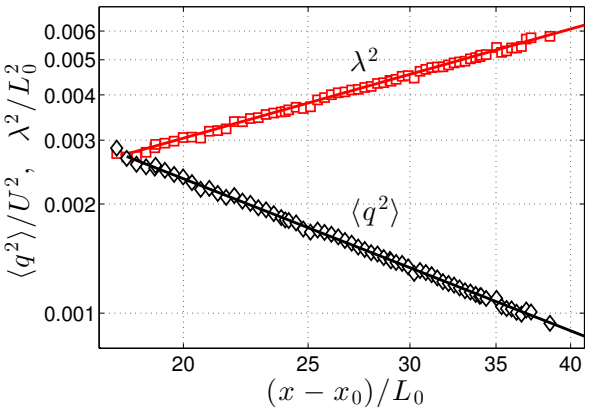

(a)

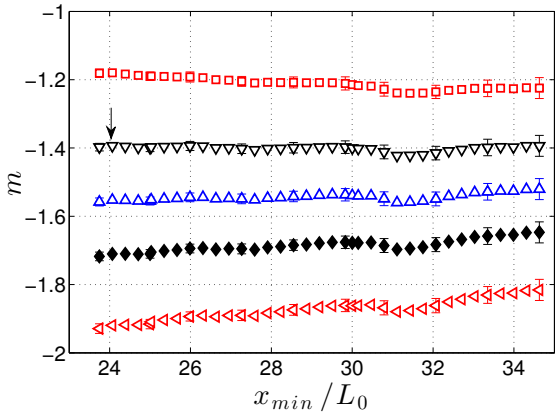

(b)

Figure 3. (a) The decay of turbulent kinetic energy and evolution of the Taylor microscale with power-law fits. (b) Variations of m with $x_{\min}/L_0$; (□) $x_0/L_0 = 10$, (▽) $x_0/L_0 = 6$, (△) $x_0/L_0 = 3$, (♦) $x_0/L_0 = 0$, (◁) $x_0/L_0 = -4$. An arrow indicates the algorithm's chosen solution.

Self-similarity of the spectra

Typically for HIT, when normalized by large scale variables, L_u and $\langle u^2 \rangle$, the spectra ($\langle u^2 \rangle = \int_0^\infty F_{11}(k)\mathrm{d}k$) should collapse only at the low wavenumbers. The opposite is true when normalized by Kolmogorov variables, η and ν, e.g. Antonia & Orlandi (2004). This is a consequence of Richardson-Kolmogorov phenomenology, which predicts that there are two sets of variables, inner and outer, that collapse the high- and low-frequency parts of the spectra, respectively. Figure 4 demonstrates that these trends are true of the data collected here. In each plot, spectra are shown for three downstream locations and their collapse is as one would expect for a regular grid. This agrees with the findings of Krogstad & Davidson (2011) and contrasts with the findings of Mazellier & Vassilicos (2010) and Valente & Vassilicos (2011) who found that normalization by large scale variables collapsed the spectra for all k.

Although this result is expected, it is significant because it contrasts with previous measurements behind fractals that showed evidence of a self-preserving single-length-scale form of turbulence (Mazellier & Vassilicos, 2010; Valente & Vassilicos, 2011). In these measurements, it was shown that normalization by L_u and $\langle u^2 \rangle$ resulted in approximate collapse of the spectra at all wavenumbers. Valente & Vassilicos (2011) also measured $L_u \propto \lambda$, which led them to speculate that there was a breakdown of the traditional $Re_\lambda \propto L_u/\lambda$ scaling. Figure 5(a) shows that L_u is not proportional to λ in the present measurements. Furthermore, figure 5(b) demonstrates that the $Re_\lambda \propto L_u/\lambda$ scaling is preserved. This key difference between the present measurements and previous measurements is likely the cause for the difference in the spectral scaling.

Normalized energy dissipation rate

Following from Richardson-Kolmogorov phenomenology, the dissipation is expected to scale with $\varepsilon \sim \langle q^2 \rangle^{3/2}/L_u$. This is often measured in experiments using

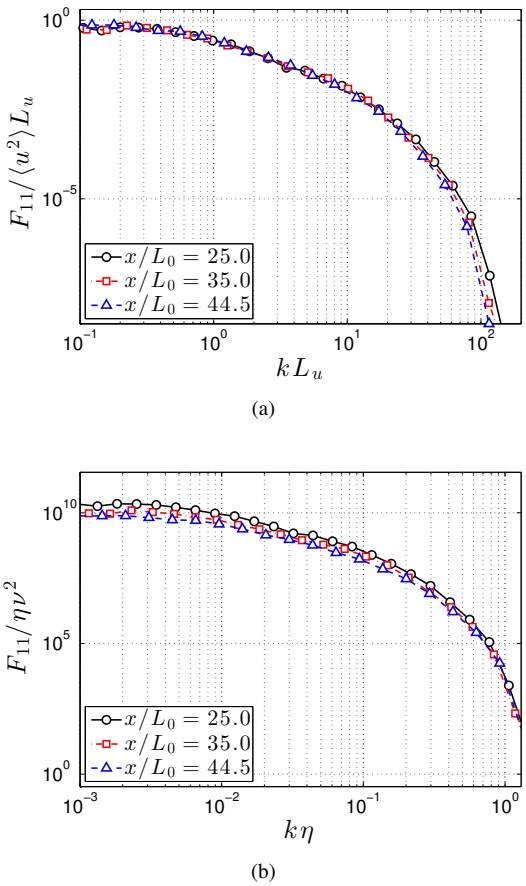

Figure 4. Spectra at three downstream locations normalized by (a) large scale variables, and (c) Kolmogorov variables.

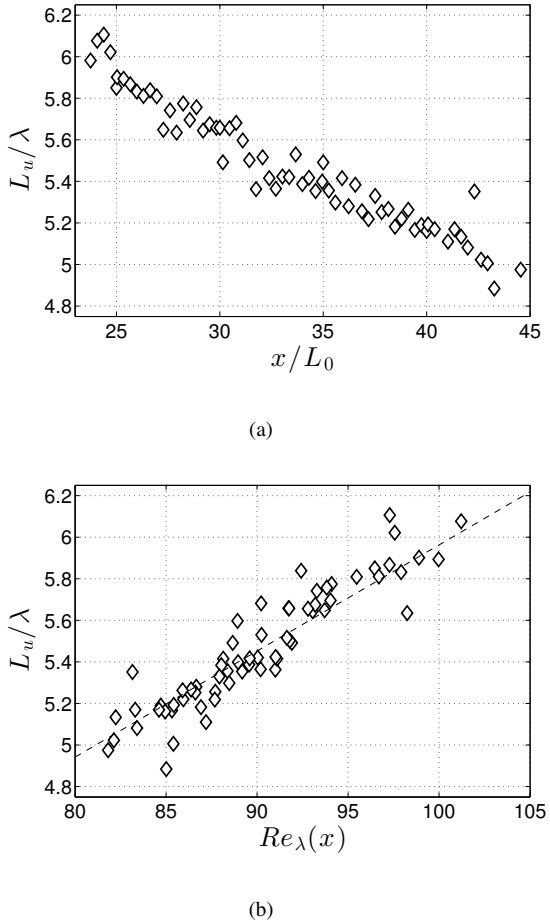

Figure 5. Evolution of L_u/λ with (a) x/L_0, and (b) Re_λ with linear fit representing $Re_\lambda \propto L_u/\lambda$.

the isotropic form of the normalized energy dissipation rate,

$$C_\varepsilon = \frac{\langle\varepsilon\rangle L_u}{\langle u^2\rangle^{3/2}}. \tag{3}$$

Anisotropy can be considered in the estimation of C_ε by using a definition of $\langle\varepsilon\rangle$ that considers both u and v and by substituting $\langle u^2\rangle^{3/2} = (\langle q^2\rangle/3)^{3/2}$. The dissipation estimated from the decay of turbulent kinetic energy, $\langle\varepsilon\rangle_d$, is calculated using the power-law fit to $\langle q^2\rangle$. The dissipation is also estimated using the isotropic definition, $\langle\varepsilon\rangle_{iso}$, and homogeneous assumptions with a X-wire, $\langle\varepsilon\rangle_{XW}$. The three different estimates of $\langle\varepsilon\rangle$ used here are defined in table 1.

In grid turbulence, $C_\varepsilon \approx$ constant with x/L_0 if Re_λ is adequately high (Sreenivasan, 1984; Burattini *et al.*, 2005). However, Valente & Vassilicos (2011) measured non-constant C_ε for their fractals and linked this to the constancy of L_u/λ and a possible breakdown of the classical $\varepsilon \sim \langle q^2\rangle^{3/2}/L_u$ scaling. Figure 6 shows C_ε estimated with both isotropic and anisotropic forms for the present measurements. The C_ε results of Valente & Vassilicos (2011) were digitized and also shown in figure 6 for comparison. For the present measurements, C_ε is approximately constant for $x/L_0 > 25$. This is not surprising given figure 5 that shows $Re_\lambda \propto L_u/\lambda$, which supports $\varepsilon \sim \langle q^2\rangle^{3/2}/L_u$ scaling. These results are once again in good agreement with previous regular grid experiments.

CONCLUSIONS

Using a novel square-fractal-element grid, measurements were conducted farther downstream of the fractal geometry than previously attainable. In this extended downstream region, it was found that a classical power-law decay region exists with $m = -1.39$ based on $\langle q^2\rangle$. The power-law decay region was also found to begin at $24L_0$. These results, both for m and the start of the power-law decay region, are in good agreement with regular grid turbulence results from the literature if L_0 is taken to be equivalent to M. It was also found that Richardson-Kolmogorov phenomenology, i.e. inner and outer variable spectral scaling, $C_\varepsilon \approx$ constant, and $Re_\lambda \propto L_u/\lambda$, was preserved in the present investigation.

While these results contrast with those of Vassilicos and co-workers for space-filling square fractals, it must be emphasized that the investigation regions of the two studies did not overlap, i.e. this study was conducted farther downstream relative to L_0. Furthermore, the Re_λ investigated here are in the range $80 < Re_\lambda < 100$, while previous fractal work has reached $Re_\lambda \approx 350$. Nonetheless, the major conclusion from this work is that the present results are in good agreement with those previously obtained using regular grids and multi-scale cross grids. This suggests that the fractal nature of the grid may not necessarily play as important a role in the decay of turbulence as previously suspected, provided the turbulence has had an opportunity to fully develop some distance downstream of the grid.

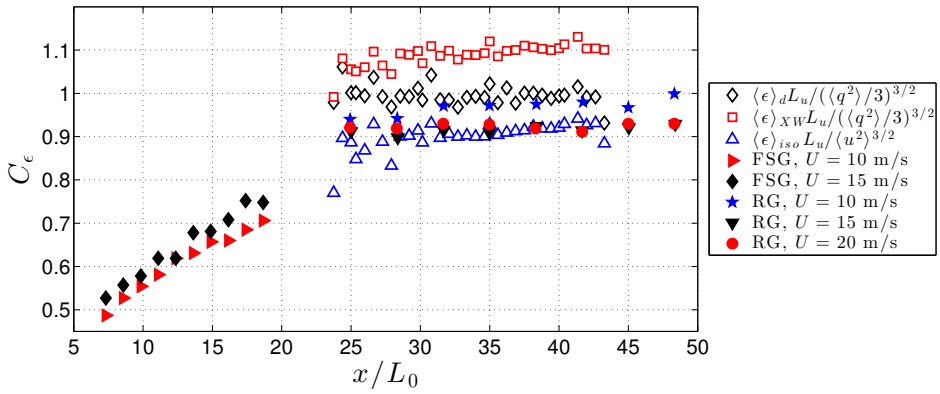

Figure 6. Normalized energy dissipation rate, C_ε, for present data estimated with three different methods (open symbols); only every second point is plotted to reduce clutter. Digitized C_ε data from Valente & Vassilicos (2011) (closed symbols) for a Fractal Square Grid (FSG), $L_0 = 237.8$ mm, and a Regular Grid (RG), $L_0 = 60.0$ mm.

Acknowledgements

The authors would like to acknowledge the financial support of the Natural Sciences and Engineering Research Council of Canada (NSERC), and the valiant efforts of Mr. R. Santos Baptista and Mr. J. Rajasekaran who aided in preparing the fractal element grid for experimentation.

REFERENCES

Antonia, R. A. & Orlandi, P. 2004 Similarity of decaying isotropic turbulence with a passive scalar. *J. Fluid Mech.* **505** (123-151).

Burattini, P. & Antonia, R. A. 2005 The effect of different X-wire calibration schemes on some turbulence statistics. *Exp. Fluids* **38**, 80–89.

Burattini, P., Lavoie, P. & Antonia, R. A. 2005 On the normalized turbulent energy dissipation rate. *Phys. Fluids* **17** (098103).

Comte-Bellot, G. & Corrsin, S. 1966 The use of a contraction to improve the isotropy of grid-generated turbulence. *J. Fluid Mech.* **25** (4), 657–682.

Corrsin, S. 1963 Turbulence: experimental methods. In *Handbuch der Physik* (ed. S. Flügge & C.A. Truesdell), pp. 524–89. Springer.

Danaila, L., Anselmet, F. & Antonia, R. A. 2002 An overview of the effect of large-scale nonhomogeneities on small-scale turbulence. *Phys. Fluids* **14**, 2475–2484.

George, W. K. 1992 The decay of homogeneous isotropic turbulence. *Phys. Fluids* **4** (7), 1492–1509.

Hearst, R. J., Buxton, O. R. H., Ganapathisubramani, B. & Lavoie, P. 2012 Experimental estimation of fluctuating velocity and scalar gradients in turbulence. *Exp. Fluids* **53**, 925–942.

Hurst, D. & Vassilicos, J. C. 2007 Scalings and decay of fractal-generated turbulence. *Phys. Fluids* **19** (035103).

Krogstad, P.-A. & Davidson, P. A. 2010 Is grid turbulence Saffman turbulence? *J. Fluid Mech.* **642**, 373–394.

Krogstad, P.-A. & Davidson, P. A. 2011 Freely decaying, homogeneous turbulence generated by multi-scale grids. *J. Fluid Mech.* **680**, 417–34.

Krogstad, P.-A. & Davidson, P. A. 2012 Near-field investigation of turbulence produced by multi-scale grids. *Phys. Fluids* **24** (035103).

Lavoie, P., Djenidi, L. & Antonia, R. A. 2007 Effects of initial conditions in decaying turbulence generated by passive grids. *J. Fluid Mech.* **585**, 395–420.

Mazellier, N. & Vassilicos, J. C. 2010 Turbulence without Richardson-Kolmogorov cascade. *Phys. Fluids* **22** (075101).

Mi, J., Xu, M. & Du, C. 2011 Digital filter for hot-wire measurements of small-scale turbulence properties. *Meas. Sci. Tech.* **22** (125401).

Mohamed, M.S. & LaRue, J.C. 1990 The decay power law in grid-generated turbulence. *J. Fluid Mech.* **219**, 195–214.

Sreenivasan, K. R. 1984 On the scaling of the turbulence energy dissipation rate. *Phys. Fluids* **27** (5), 1048–1051.

Valente, P. C. & Vassilicos, J. C. 2011 The decay of turbulence generated by a class of multiscale grids. *J. Fluid Mech.* **687**, 300–340.

Wang, H. & George, W. K. 2002 The integral scale in homogeneous isotropic turbulence. *J. Fluid Mech.* **459**, 429–443.

Wyngaard, J. C. 1968 Measurements of small-scale turbulence structure with hot wires. *J. Sci. Instr.* **1** (2), 1105–1108.

Zhu, Y. & Antonia, R. A. 1995 Effect of wire separation on X-probe measurements in a turbulent flow. *J. Fluid Mech.* **287**, 199–223.